POLITECNICO DI TORINO
Repository ISTITUZIONALE

Uniaxial Tensile Tests and Digital Image Correlation Analysis for the Mechanical Characterization of Human Fascia Lata Under Different Decellularization Treatments

Original
Uniaxial Tensile Tests and Digital Image Correlation Analysis for the Mechanical Characterization of Human Fascia Lata Under Different Decellularization Treatments / Demontis, F., Loi, G., Mazzotti, E., Rodriguez Reinoso, M., Vecchio, F., Faini, A.C., Leone, A., Camusso, E., Genzano Besso, F., Surace, C., Lacidogna, G., Scaramozzino, D.. - In: JOURNAL OF BIOMEDICAL MATERIALS RESEARCH. PART A. - ISSN 1549-3296. - STAMPA. - 113:11(2025), pp. 1-13. [10.1002/jbm.a.38012]

Availability:
This version is available at: 11583/3005004 since: 2025-11-07T23:12:46Z

Publisher:
John Wiley and Sons

Published
DOI:10.1002/jbm.a.38012

Terms of use:

This article is made available under terms and conditions as specified in the corresponding bibliographic description in the repository

Publisher copyright
Wiley postprint/Author's Accepted Manuscript

This is the peer reviewed version of the above quoted article, which has been published in final form at http://dx.doi.org/10.1002/jbm.a.38012.This article may be used for non-commercial purposes in accordance with Wiley Terms and Conditions for Use of Self-Archived Versions.

(Article begins on next page)

11 November 2026

Title: Uniaxial tensile tests and Digital Image Correlation analysis for the mechanical characterization of human Fascia Lata under different decellularization treatments

Short title: Mechanical characterization of Fascia Lata

Authors:

Francesca Demontis[1,$], Giulia Loi[1,$], Edoardo Mazzotti[1,$], Mariana Rodriguez Reinoso[1,2], Federico Vecchio[1], Angelo Corso Faini[3], Agnese Leone[4], Elisa Camusso[4], Federico Genzano Besso[5], Cecilia Surace[1,2], Giuseppe Lacidogna[1], Domenico Scaramozzino[1,6,*]

Affiliations:

[1]Department of Structural, Geotechnical and Building Engineering, Politecnico di Torino, Torino, Italy. [2]BIO MAterials & STructures (BIOMAST) Laboratory, Politecnico di Torino, Torino, Italy. [3]Department of Medical Sciences, Università degli Studi di Torino, Torino, Italy. [4]Banche dei Tessuti e Bioconservatorio, Azienda Ospedaliera Universitaria Città della Salute e della Scienza di Torino, Torino, Italy. [5]Centro Regionale Trapianti, Azienda Ospedaliera Universitaria Città della Salute e della Scienza di Torino, Torino, Italy. [6]Currently affiliated with: Department of Oncology-Pathology, Karolinska Institutet, Solna, Sweden.

[$]These authors contributed equally.

*Corresponding author: domenico.scaramozzino@polito.it; domenico.scaramozzino@ki.se

ha formattato: Colore carattere: Testo 1

ha formattato: Colore carattere: Testo 1

Acknowledgments

We acknowledge “Banca dei Tessuti Muscoloscheletrici di Torino” for providing the FL samples (resulted not eligible for transplant) from human donors, and the Department of Structural, Building, and Geotechnical Engineering (Politecnico di Torino) for providing the facility and equipment to carry out mechanical tests.

Data Availability

All the macro-mechanical data as well as movies of DIC strain maps are freely available on *figshare* at https://doi.org/10.6084/m9.figshare.29626358.

ha formattato: Colore carattere: Testo 1

Funding

This research did not receive any specific grant from funding agencies in the public, commercial, or not-for-profit sectors.

Abstract

Fascia Lata (FL) is frequently employed as a graft source in reconstructive surgery. To minimize unwanted responses from the host immune system, several decellularization treatments have been proposed. Effective treatments should aim at avoiding the deterioration of the physical and mechanical properties of the implanted tissue. In this work, we carried out a mechanical characterization of FL specimens from human dead donors, both in their native-physiological condition and upon decellularization with three commonly used detergents, t-octyl-phenoxypolyethoxyethanol (Triton X-100), sodium dodecyl sulfate (SDS), and tri-n-butyl phosphate (TnBP). Uniaxial tensile tests were used to characterize the elastic stiffness and ultimate stresses of the tissue, and Digital Image Correlation (DIC) was applied to monitor the strain evolutions and meso-mechanical deformation responses. None of the investigated decellularization protocols was found to lead to a significant deterioration of the FL mechanical properties, suggesting the applicability of these chemical treatments for graft preparation and usage in the clinical practice. The application of DIC also allowed us to get a first estimate of the FL Poisson ratio as well as to draw the attention on the inhomogeneity of strain distributions, suggesting that the use of average engineering strains can lead to an oversimplification of the actual deformation field.

Keywords: Biomechanics, grafting material, decellularization, human Fascia Lata, uniaxial tensile test, Digital Image Correlation.

1. Introduction

The large amounts of surgical reconstructive procedures due to soft tissue traumatic injuries, acquired or iatrogenic defects, represent a significant health and economic burden. Generally, these procedures require the employment of autologous or allogenic grafts[1]. Fascia Lata (FL) has received particular attention within the medical community since it represents a validated graft source and has been adopted in several types of reconstructive procedures[2]. FL grafts have been used as support in facial paralysis[3] and facial reanimation[4], for closure of enlarged tracheoesophageal punctures after laryngectomy-laryngopharyngectomy surgeries[5], penile[6] and pelvic[7] reconstruction, ophthalmic plastic and reconstruction surgery[8], reconstruction of full-thickness chest walls[9], rhinoplasty interventions[10], etc.

Biological graft materials are made of abundant extracellular matrix (ECM) and they generally need to undergo specific manufacturing methods that remove cellular and major histocompatibility complex components[11]. These methods include decellularization and chemical crosslinking to remove antigenic epitopes, DNA, and other biomolecules, while trying to minimize negative effects on the ECM features[12,13]. Decellularization methods remove cells while preserving the ECM using chemical, enzymatic, and physical approaches, and encompass a wide variety of detergents, concentrations, and incubation times. The most common chemical-enzymatic decellularization methods make use of chemical detergents such as sodium dodecyl sulfate (SDS), t-octyl-phenoxypolyethoxyethanol (Triton-X 100), tri-n-butyl phosphate (TnBP), enzymes, etc.[1]. SDS is an ionic detergent and one of the most potent reagents for clearing cellular material and DNA, but it has the potential to denature proteins and weaken collagen, and it is difficult to wash out completely. In comparative work on human, mouse and porcine tissues, SDS was observed to remove donor DNA more efficiently than sodium deoxycholate but at greater cost to ECM preservation[14,15]. Extensive rinsing with a milder detergent is often required afterwards. Triton X-100 is a non-ionic detergent, disrupts lipid–lipid and lipid–protein interactions, while better maintaining ultrastructure and growth factors. It is generally less effective than SDS at removing cells and is suboptimal for tissues rich in glycosaminoglycans (GAGs) and lipids, yet it has been widely applied across soft tissues and has been part of several successful protocols[16,17]. TnBP is typically classified among zwitterionic/organic solvent decellularizers and can match SDS in cell removal while better preserving ECM architecture. This has been shown in porcine tendon and ligament tissues[18], and in human saphenous vein when paired with Triton X-100 and DNase[19]. More broadly, zwitterionic agents (e.g., CHAPS, SB-10/SB-16) often strike a balance between cell clearance and ECM preservation. Besides these reagents, others have been studied such as chelators, i.e., EDTA/EGTA, which aid cell detachment by binding divalent cations and cytotoxins like latrunculin, disrupting actin–myosin. On the other hand, other non-chemical methods can include extreme pH solutions (which carry the risk of degrading growth factors and mechanical properties), alcohols such as ethanol and methanol (which dehydrate and solubilize lipids but may stiffen tissues), enzymes such as trypsin, dispase, DNase, RNase, phospholipase A2, etc., as well as physical methods like freeze–thaw cycles, agitation, pressure, sonication, and supercritical CO_2[20].

The *in vivo* biodegradability of the ECM plays a key role in determining the host immune response and the remodeling processes inducing the clinical outcome[13,21], thus constituting a driving factor for the choice of the optimal decellularization protocol. However, it is crucial that the implanted grafting material is also appropriate from a mechanical point of view[22]. Since the implanted graft is expected to withstand physiological loads, adequate mechanical strength and elasticity are necessary to allow

mechanical loads to be correctly sustained by the surrounding tissues, while undergoing proper deformations and minimizing localized strains. Therefore, it is pivotal to properly characterize the mechanical behavior of the native tissue and how this is impacted by decellularization treatments.

Fascia Lata is an aponeurotic fascia, which encloses the tight muscles, and it is a dense and regular connective tissue with a multilayered organization, with collagen fibers disposed in each layer along specific directions. A comprehensive review of the mechanical characterization of human FL tissues can be found in a recent paper from Bonaldi et al[23]. Almost one century ago, Gratz et al. reported the first results arising from uniaxial tensile tests on human FL, assessing its ultimate strength and elasticity with different specimen arrangements[24,25]. Linear stiffness and elastic modulus of human samples under uniaxial tests were also investigated by Derwin et al.[26], where the biomechanical properties of the tissue were studied in untreated, decellularized, and antibiotic-treated samples. Biaxial tests were performed by Eng et al.[27] and Pancheri et al.[28] to investigate the strength and stiffness of FL samples from adult goats, both in the longitudinal and transverse direction with respect to the orientation of collagen fibers. These tests confirmed that the material exhibits a strong anisotropic behavior, with higher stiffness in the longitudinal direction[27,28]. A comprehensive analysis of the mechanical behavior of human FL, also considering site specificity and gender differences, was carried out by Otsuka et al.[29], who studied variabilities in stiffness, Young's modulus, and hysteretic behavior in different samples. Pukšec et al.[30] investigated the stress-strain characteristics of FL from fresh human dead donors, and compared them to those obtained from the muscle fascia and the dura mater. More recently, de Campos Azevedo compared the biomechanical properties of proximal and mid-thigh FL samples[31], and Bonaldi et al.[32] highlighted the strong anisotropic response with respect to the principal collagen fiber direction, also proposing a new constitutive model able to mimic intra- and interlayer interactions. All the studies reported above are characterized by large result variances[23], which is mainly due to the: (1) intrinsic variability of the biological tissue; (2) different origin species (humans, goats, sheep) and specimen preparations; (3) different testing and experimental conditions, e.g., type of loading (uniaxial vs. biaxial, static vs. cyclic), speed of traction, gripping conditions to the loading device, etc.

Besides standard tensile tests, a few of the studies reported above also showed the use of complementary techniques which helped to interpret and integrate the tensile results, such as computer modeling (finite element method, analytical models) and full-field strain measurements. In particular, Digital Image Correlation (DIC) is an optical technique which allows to capture the displacements and strains of a surface under direct or indirect loadings. It is based on the application of a speckled pattern that is recognized by digital cameras and used for the assessment of the displacement field evolution through image-correlation algorithms[33]. This allows to investigate the full-field strain properties of the specimen, which is crucial in highly inhomogeneous materials such as biological samples. In recent years, DIC has found increasing application in biomechanics[34], e.g., for the investigation of bovine cornea under constrained inflation conditions[35], for the determination of strains in excised larynx vocal folds[36], for the three-dimensional strain analysis of human tendons[37], etc. A few years ago, Sednieva et al.[38] made use of DIC together with motion analysis to assess the *in situ* strain evolution of FL during leg movement in three human dead donors. To the best of our knowledge, this was the only application of DIC to characterize deformation ranges of FL tissues, although not up to ultimate failure. In this work, we report the results of a mechanical investigation on human FL samples under uniaxial tension up to final collapse, complemented by DIC analysis, also exploring the impact that different chemical protocols have on the mechanical properties of the tissue.

2. Materials & Methods

2.1. Preparation of native FL specimens

Due to the unsteady availability of FL samples from human dead donors suitable for research purposes mechanical tests were carried out in five separate experimental campaigns, i.e., in October 2020, January 2021, April 2021, February 2022, and May 2022. The use of these human tissues for mechanical characterization purposes and for assessment of our decellularization protocols (see below) was carried out in compliance with our national guidelines. Information about age, sex, cause of death, and reason for transplant ineligibility of the three donors are reported in Table S1 in the Supplementary Material. All FL tissues were carefully harvested from the mid-lateral regions of both thighs in the operating room and placed for ~10 minutes into a sterilized container filled with 10 liters of sanitizer at 5% concentration to reduce the risk of microbial contamination. After assessing that the tissue had not been contaminated before or during the removal, all samples were frozen at –80 °C, thawed the day before the mechanical tests, and then left at room temperature (Figure 1a). The tissues were then cut into rectangular samples (Figure 1b), so that the longer side followed the main direction of collagen fibers. We managed to collect a total of sixteen rectangular specimens from native FL, which were analyzed in the five experimental campaigns (see Table S2 in the Supplementary Material). The dimensions of the specimens were carefully measured via a digital caliber (for the width) and a digital micrometer (for the thickness). Several measurements on different points of the specimens were carried out, so that mean and standard deviation values of the geometrical dimensions were extracted. The cross-sectional areas of the samples, needed for stress calculations, were computed based on width and thickness values, applying the propagation of standard deviation errors (see Table S2). The initial length L_0 of the sample was evaluated as the distance between the clamps in the testing machine at the beginning of the test (see Section 2.3).

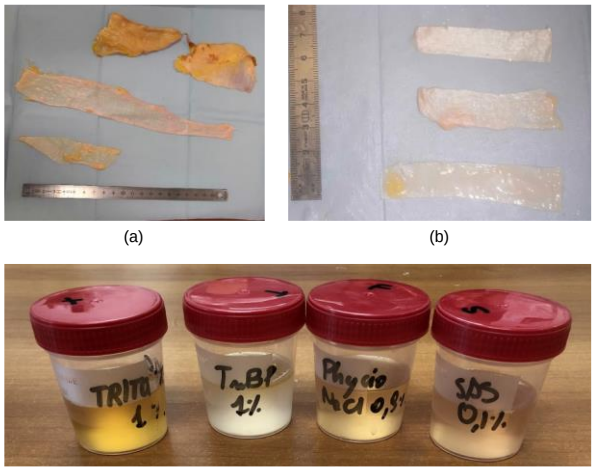

Figure 1. (a) Human Fascia Lata (FL) tissue from which individual specimens were collected; (b) picture of the rectangular specimens for the uniaxial tensile test; (c) a picture of the three different solutions for decellularization (Triton X-100, SDS, TnBP), plus the physiological solution.

2.2. Decellularization protocol and preparation of decellularized FL specimens

The chemical protocols for FL decellularization were designed based on the architecture of the native tissue, as suggested by Blaudez et al.[1], to obtain suitable levels of DNA removal without causing significant damages to the ECM. The chemical agents employed in this study for the decellularization of FL tissues were Triton-X100, SDS, and TnBP. For each agent, we considered a total of six FL samples for the mechanical investigation (four were tested in February 2022 and two in May 2022, see Table S3 in the Supplementary Material). All samples were soaked in three different solutions (Figure 1c), in combination with 0.1% ethylenedinitrilotetraacetic acid (EDTA) and deionized water for 24 hours at room temperature (20 °C): (1) 1% solution of Triton X-100; (2) 0.1% solution of SDS; (3) 1% solution of TnBP. Afterwards, all specimens underwent 2 cycles of PBS (phosphate buffered saline) washes for 30 minutes. The creation of rectangular specimens for the mechanical tests (Figure 1b), as well as the measurement of their geometrical characteristics, were carried out following the same approach reported above.

2.3. Uniaxial tensile tests

All specimens were tested under uniaxial tensile tests to evaluate their macro-mechanical properties (Figure 2a). The tests were performed using an MTS Insight® Electromechanical Testing Systems tensile machine, with a 1000 N load cell and sensitivity of 2.164 mV/V. All samples were installed into 200N-loaded pneumatic clamps with knurling, and small gauze pads were inserted between the FL surfaces and the clamps in order to absorb the liquid released by the tissue, increase friction, and reduce the risk of slippage. The tensile tests were carried out using displacement control conditions, with a displacement rate of 0.1 mm/s and a sampling frequency of 30 Hz. The Young's

(elastic) modulus E was calculated as the slope of the linear elastic region in the stress-strain curves. The initial and final values of the linear elastic region were automatically detected by the TESTWORKS® software of the testing machine. As mentioned above, the initial length of the specimens L_0, used to compute the average engineering strain, was considered as the initial distance between the two clamps (see Figure 2b). After the tensile tests, macro-mechanical properties such as elastic modulus E and maximum stress σ_{max} were evaluated also considering propagation of uncertainties from the geometrical dimensions (see Supplementary Material).

Preconditioning is often employed in the mechanical testing of soft tissues to encourage initial alignment of collagen fibers along the primary loading direction, thereby enhancing reproducibility and reducing experimental variability. However, this practice is not commonly adopted for human FL samples, and when it is used, protocols vary significantly across studies[23]. As further highlighted in a recent systematic review on the mechanical properties of ligaments, preconditioning procedures greatly differ in terms of number of cycles, strain amplitude, and applied forces, and there is no consensus on standardized protocols across tissues and species[39]. Moreover, preconditioning may introduce permanent structural changes in the tissue, potentially altering the measured mechanical properties, and its repeated cycles can induce micro-damage or even rupture. In studies with a limited number of samples, such as the present one, this may ultimately prevent a meaningful statistical analysis. Furthermore, here we also implemented Digital Image Correlation (DIC) on a subset of specimens (see below), where preconditioning could have introduced unwanted deformations in the speckle pattern, potentially compromising strain measurements during subsequent testing. For all these reasons, we chose not to precondition any of our FL samples. Instead, specimens were carefully sectioned along the dominant collagen fiber direction (Figure 1b), and we verified that samples cut in this orientation exhibited substantially higher maximum stress and stiffness compared to those cut transversely (Figure S1), consistent with findings reported in previous studies[23,29].

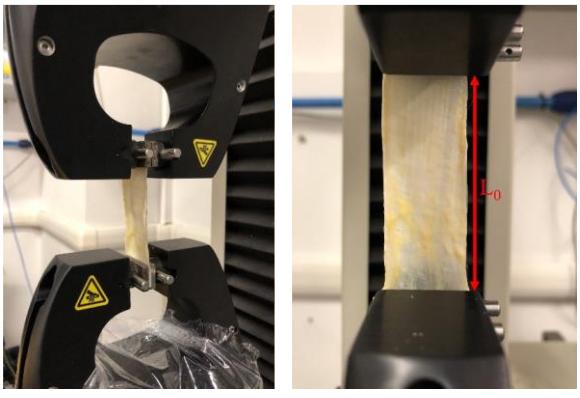

Figure 2. (a) Uniaxial tensile test of a FL sample; (b) measurement of the initial distance L_0.

2.4. Digital Image Correlation (DIC) analysis

In combination with the tensile tests, Digital Image Correlation (DIC) was used to monitor the strain distribution in a few samples. For the DIC analysis, we investigated the displacement fields in

Nat J4, TRX F4, SDS F3, and TnBP F3 specimens (see Tables S2 and S3 in the Supplementary Material for specimen labels). The DIC method was implemented with the VIC-EDU System, an optical non-contact method that can measure surface displacements. This enables the visualization of strain maps and deformation vector fields in all the directions, thus granting the characterization of inhomogeneous and anisotropic responses in complex specimens such as biological tissues[34–37]. A random paint pattern was applied on each sample (Figure 3a), by using a speckled pattern tool embedded with black water-based ink. The speckle size was chosen to fit in a desirable range of 1-5 pixels[34]. Subsequently, a series of images of the specimen undergoing uniaxial deformation was acquired. The software VIC-3D was used to calculate the strains between any two points within the area covered by the speckle pattern using virtual extensometers placed along the surface.

The VIC-EDU System was placed 54.5 cm away from the specimen (Figure 3b). A three-dimensional configuration was used to compensate for possible out-of-plane displacements during testing. For better lighting of the specimen surface, two lights were added to the LED light integrated in the system. The VIC-Snap acquisition software was used to monitor the view field of the cameras and verify the good placement of the specimen and optimal lighting. The position of the lights was changed until the optimal lighting (50 ms of exposure time) was verified for all tested specimens. Images were acquired with two monochrome cameras, FLIR Blackfly® U3-23S6M-C, with a progressive scan CMOS 1/1.2" image sensor, SONY IMX249. The resolution of the acquisition was 2.3 Megapixels, 1920 x 1200 pixels, with 5.86 x 5.86 µm pixel size. The system was calibrated by taking 30 images of the pattern calibration plate with different positions and orientations. During the test, both cameras were set to capture an image either every 2 or 3 seconds. For the post-processing in VIC-3D, an area of interest was defined for each sample and divided into smaller subsets of a size large enough to contain sufficient pattern information with minimal overlap. Due to the small dimension of the speckle, the size of the subsets was set to 9 and the step size that controls how many pixels are apart from each data point was set to 1. The reference point to enable the full-field displacement correlation was finally set in a position close to the lower grips.

(a) (b)

Figure 3. (a) Speckle pattern on a FL specimen; (b) integrated tensile test and DIC experimental setup.

3. Results

3.1. Uniaxial tensile tests

The results of the mechanical tensile tests of all FL samples are reported in Tables S4-S6 in the Supplementary Material. Figure S2 shows the full force-displacement curves obtained by the testing machine for all specimens divided per treatment type, i.e., native, treated with Triton X-100, SDS, and TnBP. All samples were found to exhibit a pronounced softening behavior in the post-peak regime with no fragile collapse: after reaching the maximum load all samples allowed to accommodate higher displacements for lower load intensities before reaching ultimate failure (Figure S2). While for several specimens this was found to occur because of the capability of the tissue to redistribute tensile stresses across the collagen fiber network after the first fibers start to break, for some samples this was a consequence of large deformations/lacerations close to the machine clamps, highlighting a weakening of the tissue regions close to the external constrains. Force-displacements curves were then converted into stress-strain relationships, by considering the geometrical properties of each sample (cross-sectional area A and initial length L_0), and are reported in Figure 4. Since a comparison in terms of stresses and strains in the post-peak regime is meaningless for our purposes, for clarity Figure 4 reports the stress-strain curves only up to the maximum stress σ_{max}. A large variability across the FL samples was observed both in terms of stresses, strains, and stiffnesses (slopes of the curves), which is a typical fingerprint of the intrinsic variability of biomaterials[23,40].

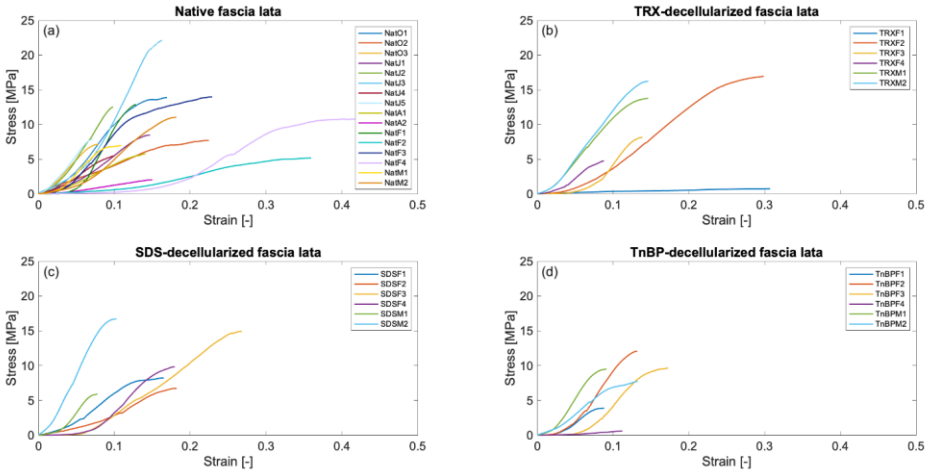

Figure 4. Stress-strain curves (up to σ_{max}) for all FL specimens: (a) native samples; (b) samples treated with Triton X-100; (c) treated with SDS; (d) treated with TnBP. The colors of the curves refer to the different samples investigated during the various experimental campaigns (see Tables S2-S6 in the Supplementary Material for details about specimen labels). The full force-displacement curves, also including the post-peak regime, are reported in Figure S2.

Ensuring a proper mechanical rigidity for small deformations is pivotal to redistribute mechanical loads in physiological conditions, and the elastic modulus is a straightforward metric to quantify the

material rigidity in the small-deformation regime. Figure 5a shows a comparison between the computed elastic moduli E across the population of all FL samples, colored according to the treatment protocol (native FL, treated with Triton X-100, SDS, TnBP). The elastic modulus was found to range from a minimum of ~4 MPa to a maximum of ~250 MPa, with an average value of ~115 MPa. Despite the large variations, these values are in agreement with previous investigations on human samples[23,29,31,32]. A similar variability was also found for maximum stresses σ_{max}, whose values are reported in Figure 5b. These were found to range from a minimum of ~0.6 MPa to a maximum of ~22 MPa, with an average value of ~10 MPa. Also these values are in agreement with some previous analyses[23,32]. A clear positive correlation was observed between these two macro-mechanical properties, E and σ_{max} (see Figure S3 in the Supplementary Material), i.e., we generally found that stiffer samples (higher E) are also the ones that are able to withstand higher loads (higher σ_{max}). A Pearson correlation coefficient between E and σ_{max} values of ~0.7 was obtained across the whole dataset, with significant correlations also at the level of individual treatment groups, ranging from a minimum of ~0.5 for SDS samples up to ~0.9 for TnBP ones (see Figure S3 caption).

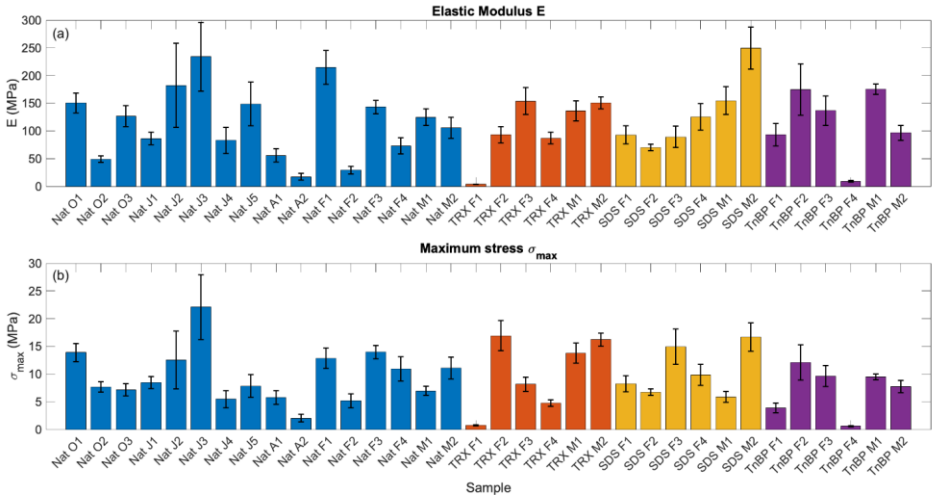

Figure 5. Comparison between (a) elastic moduli E and (b) maximum stresses σ_{max} for all FL samples (native FL group in blue, treated with Triton X-100 in red, treated with SDS in yellow, treated with TnBP in purple). For each sample, average and standard deviation values are shown (according to the values reported in Table S6 in the Supplementary Material).

To investigate the impact of the chemical treatment on the macro-mechanical properties of FL samples, we computed group-aggregated values for each FL group (native FL, treated with Triton X-100, SDS, TnBP). This is expected to average out the differences at the level of individual specimens yet taking into account the uncertainties that affects the measurement in each sample (see Supplementary Material). The results of these calculations considering the entire dataset of 34 samples seem to suggest a pronounced loss of mechanical performance when using Triton X-100 and TnBP treatments (see Table S8 and Figures S4a-S5a in the Supplementary Material). However, this is not directly observable from the data reported in Figure 5 (as well as in Table S6 and Figure S2 in the Supplementary Material), but most likely an effect coming from the low mechanical performance detected in only two samples, i.e., TRX F1 and TnBP F4, which with high probability are outliers of

the E and σ_{max} distributions (see the extremely flat stress-strain curves of TRX F1 and TnBP F4 in Figure 4). To confirm the outlier nature of these specimens, as well as to remove the influence of all outliers on group-aggregated averages, we calculated 5th and 95th percentiles of the distributions of E and σ_{max} across all samples and considered outliers all specimens exceeding these boundaries. Table S7 in the Supplementary Material reports the list of lower- and upper-limit outliers, confirming that TRX F1 and TnBP F4 are lower-limit outliers for both the E and σ_{max} distribution. We also identified three additional upper-limit outliers (Table S7), i.e., Nat J3 (>95th percentile of both E and σ_{max}), SDS M2 (>95th percentile of E), and TRX F2 (>95th percentile of σ_{max}). By removing these outliers from the group-aggregated calculations, elastic moduli and maximum stresses were found to exhibit more comparable values among the different treatment groups (see Figures S4-S5 in the Supplementary Material). Figure 6a reports aggregated values for the elastic moduli of each treatment group not considering the outliers (Nat J3, TRX F1, TRX F2, SDS M2, TnBP F4). In this case, we clearly observed that none of the decellularization method leads to a degradation of the tissue stiffness, with elastic moduli even above the average value in native samples (Figure 6a and Figures S4b-d). Similarly, Figure 6b reported the comparison in terms of σ_{max} values, showing that all treatment methods lead to a similar value of ultimate stress, around ~7 MPa (see also Figure S5b-d). These results suggest that, on average, none of the decellularization protocols investigated here (Triton X-100, SDS, TnBP) leads to a mechanical degradation of the tissue, implying that these treatments can be effectively used - at least from a mechanical point of view - in surgical reconstruction applications.

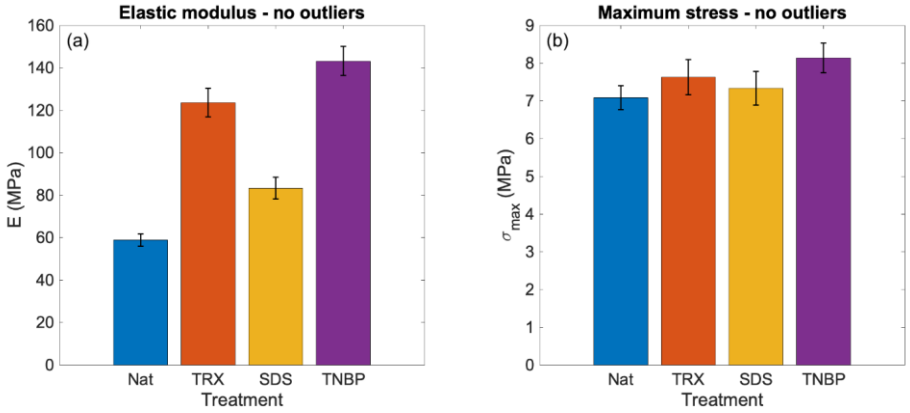

Figure 6. Values of (a) elastic moduli E and (b) ultimate stresses σ_{max}, aggregated over each treatment group (native FL group in blue, Triton X-100 in red, SDS in yellow, TnBP in purple). Average values and error bars of elastic moduli have been computed according to Eqs. (S7a-b) in the Supplementary Material and considering all samples except for the outliers (5th and 95th percentiles) in both E and σ_{max} distributions (see Table S7 in the Supplementary Material). Figures S4-S5 in the Supplementary Material show treatment-aggregated quantities for both E and σ_{max} values with different outlier groups considered.

To further substantiate that no significant differences exist in the average macro-mechanical properties among the four treatment groups, we performed a one-way ANOVA (see Supplementary Material). When applied to the full dataset, the analysis yielded p-values of ~0.91 for E and ~0.69 for σ_{max} (Table S9), indicating no statistically significant variation across the treatment groups. These findings are consistent with the trends observed in Figure 5 and the violin plots presented in

Supplementary Figure S6. Given that outliers can artificially inflate within-group variance or obscure between-group differences, we also repeated the ANOVA using a reduced dataset that excluded the five previously identified outliers. Even in this more conservative analysis, the resulting p-values remained well above the typical 0.05 significance threshold (Table S9), further reinforcing the conclusion that the applied treatments did not have a significant impact on the macro-mechanical behavior of the FL samples.

3.2. Digital Image Correlation (DIC)

To better assess the variations in strain patterns, strain deformations with DIC were quantified across a large rectangular area on the sample surface as well as within three smaller sub-regions (see Figure 7): an area close to the upper clamp (R_0-Top), close to the specimen midpoint (R_1-Center), and close to the lower clamp (R_2-Down). Furthermore, two virtual strain gauges were employed to capture directional strain components: E_1, aligned parallelly to the loading (longitudinal) direction and the collagen fibers, and E_0, aligned in the perpendicular (transverse) direction.

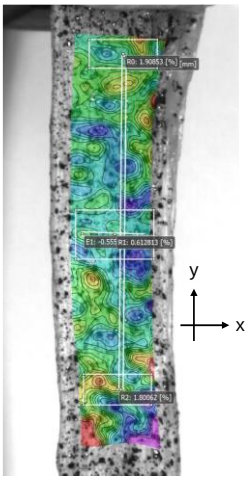

Figure 7. Example of a DIC strain map from one of the samples and position of the three smaller sub-regions (R_0-Top, R_1-Center, R_2-Down). The colors of the DIC map reflect the intensities of the measured strains. The x-y reference system for the strain calculation is also reported. The two virtual strain gauges, E_1 and E_0, used to measure longitudinal and transversal deformations respectively, are also reported.

Figure 8 illustrates the evolution of DIC longitudinal strains (e_{yy}) for the four investigated samples until maximum load σ_{max}. For each sample, the four curves refer to the different focus regions (overall surface and upper, middle, and lower are). Table S10 in the Supplementary Material also reports maximum values of e_{yy}, together with standard deviations evaluated across each sub-region. The native tissue (Nat J4) was found to exhibit an evolution of longitudinal DIC strains with maximum strain values ~5% before collapse and higher strain localizations in the lower and upper regions (Figure 8a). The sample treated with Triton X-100 (TRX F4) showed a very similar deformative response compared to the native sample but with slightly lower strain values (~4%) and a more

homogeneous strain distribution across the three sub-regions (Figure 8b). Note that Nat J4 and TRX F4 were found exhibit very similar values of macro-mechanical properties (~85 MPa for *E*, ~5 MPa for σ_{max}; see Table S6 in the Supplementary Material). The similar meso-mechanical response observed through DIC confirms the analogous mechanical-deformative behavior of these samples regardless of the chemical treatment. On the contrary, the sample treated with SDS (SDS F3) was found to exhibit a different behavior with an ultimate collapse occurring at larger DIC strains (~15%) and a medium amount of inhomogeneity in the strain localizations (Figure 8c). Note that the elastic modulus of this sample was found to be very similar to the elastic moduli of Nat J4 and TRX F4 (~85 MPa), while its ultimate stress was three times higher (~15 MPa; see Table S6). This suggests that the SDS-treated sample has a similar elastic behavior as Nat J4 and TRX F4, but a higher capability to accommodate larger longitudinal strains before failure. Finally, the sample treated with TnBP (TnBP F3) was found to show an intermediate response compared to the three other specimens, with a strain evolution pattern similar to the native and TRX samples but at slightly higher strain values (~7%, Figure 8d). Note that this sample was found to have a much higher elastic modulus (~140 MPa), but a somewhat intermediate value of ultimate stress (~10 MPa) compared to the other three.

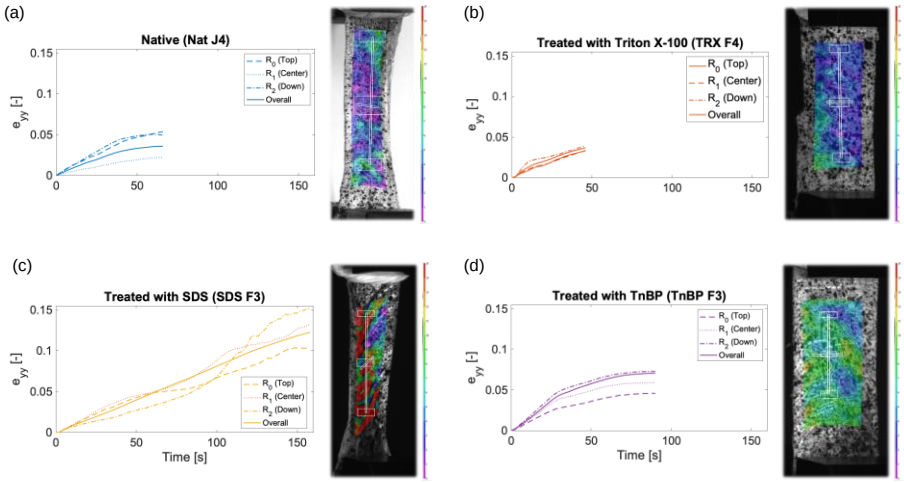

Figure 8. Time-evolution of DIC longitudinal strains (e_{yy}) in: (a) native FL specimen (Nat J4), (b) sample treated with Triton X-100 (TRX F4), (c) sample treated with SDS (SDS F3), (d) sample treated with TnBP (TnBP F3). Each graph reports values of e_{yy} deformations evaluated on the overall surface ("Overall") and on smaller sub-regions located in the upper (R_0), middle (R_1), and bottom (R_2) portions of the specimen (see Figure 7). Snapshots of the DIC e_{yy} deformation fields are reported close to each graph.

Table S10 in the Supplementary Material summarizes not only maximum values of longitudinal strains (e_{yy}), but also transversal (e_{xx}) and Von Mises (e_{VM}) deformations, with standard deviations across the averaging surfaces (overall, R_0, R_1, R_2). These results highlight a few differences in the maximal mesoscopic deformations detected across the samples. The native FL sample shows Von Mises strains that are quite homogeneous across the specimen surface, with peaks at ~11%. The sample treated with Triton X-100 displays maximum overall strains very similar to the native sample, with slightly lower spatial discrepancies (see also comparison between Figure 8a and Figure 8b), with

Von Mises strains slightly lower compared to the native sample (~7%). On the contrary, the sample treated with SDS undergoes larger maximum strains, both in the longitudinal and transversal direction (with peaks up to ~18%) and Von Mises strains reaching values as high as ~36%, confirming the larger deformations obtained in this sample. Finally, the sample treated with TnBP shows moderate strain values, with maximum Von Mises strains of ~10%, confirming a somewhat intermediate deformation response of this sample (Table S10).

Based on the use of the two virtual gauges E_1 and E_0 (see Figure 7), we also evaluated the maximum longitudinal and transversal elongations of the specimen, as well as the Poisson ratios at the moment of maximum longitudinal elongation at σ_{max}. As reported in Table S11 in the Supplementary Material, Poisson ratios were found to be ~0.23 for the native specimen, ~0.36 for TRX, ~0.50 for SDS, and ~0.20 for TnBP. While a number of studies have explored the anisotropic behavior of FL tissue, reporting superior mechanical properties along the primary collagen fiber direction[23,27,28,32] (see also Figure S1), and previous research has employed experimental methods to determine Poisson ratio in various soft tissues – including tendons[41–45], muscles[46,47], cartilage[48–51], vessel tissue[51] – to the best of our knowledge, this work represents the first experimental characterization of Poisson ratio in human FL tissue. Consequently, no direct values from the literature are currently available for comparison. Moreover, prior investigations have reported substantial variability in Poisson ratios. For example, values for tendons alone have ranged from negative[45] to extremely high values approaching ~3[41]. Given this context, the Poisson ratios presented here for FL tissue should only be considered preliminary estimates. Further dedicated testing under carefully controlled conditions is necessary to refine these measurements and better capture their variability. Yet, the fact that such different chemical treatments led to estimates of Poisson values of the same order of magnitude confirms that these decellularization protocols do not seem to cause any significant alteration of the mechanical properties of FL tissues at the mesoscopic (deformative) level.

4. Discussion

As mentioned in the Introduction, FL is widely used in surgery for its mechanical strength and adaptability, with applications ranging from ligament and tendon reconstruction in orthopedics, to dural repair in neurosurgery, ptosis correction in ophthalmology, and reinforcement of abdominal walls, pelvic floors, or hernia repairs in reconstructive and general surgery. Despite these advantages, its clinical use can be severely limited by immunogenicity. Using decellularization protocols can reduce antigenicity while – as we showed here – preserving the mechanical properties of the tissue. In this way, we can use less immunogenic – yet equally resistant – tissues, reducing the risk of complications such as graft degradation, fibrosis, or even rejection. Alternatives to FL are currently available as graft materials in surgery. Autologous grafts harvested from the patient, such as semitendinosus, gracilis, patellar tendon, palmaris longus, pericranium, periosteum, or dermis, offer excellent biocompatibility, but they are limited by donor site morbidity and availability. Other options are allografts from human donors which provide larger and more readily available tissue, but these may induce immune activation and related complications. Synthetic materials, including polypropylene or artificial ligaments, avoid biological variability and are widely applied in surgical procedures such as hernia repair, pelvic floor reconstruction, and some orthopedic procedures. However, they generally carry higher risks of infection, limited remodeling, or long-term failure. Compared to FL, these alternatives differ in mechanical properties, biocompatibility, and immunogenic risk. Autografts are the gold standard for biocompatibility but severely limited by donor

site morbidity, while synthetic options eliminate biological variability but carry higher risks of infection and might not always be suitable for specific surgical procedures. On the other hand, allografts such as FL provide broader availability and size flexibility, and their immunogenicity can be significantly reduced by decellularization processes, such as those used in this study.

The outcomes of our experimental investigation point out that the decellularization protocols adopted here with Triton X-100, SDS, and TnBP do not degrade the mechanics of human FL. From a purely mechanical point of view, we did not find any significant difference between the three decellularization agents, since all three led to similar mechanical performance of FL tissues and therefore could be considered equally suitable. On the other hand, from a clinical perspective, TnBP is generally considered the most suitable. While SDS is highly effective in removing cellular components, its strong cytotoxicity and the need for extensive washing steps can limit its translational potential. Triton X-100, a non-ionic detergent, has historically been used due to its gentler effect on the extracellular matrix; however, its non-biodegradable ethoxylate components have led to a progressive decline of its use in clinical-grade protocols. In contrast, TnBP combines acceptable decellularization efficiency with a favorable biocompatibility and regulatory profile, as it is already approved for viral inactivation in biomedical applications[52].

Despite the clear outcomes of our study, a few limitations of our approach need to be pointed out. First, the above conclusion holds true if outliers are removed from our group-aggregated calculations, especially the two samples TRX F1 and TnBP F4 which were found to exhibit remarkably low values of E and σ_{max} (see Figure 5). Note that TRX F2, TRX F3, and TRX F4 come from the same batch as TRX F1, and TnBP F1, TnBP F2, TnBP F3 from the same batch as TnBP F4. Therefore, the most likely explanation for such outlier behavior relies on the presence of microscopic defects in the ECM and fiber network of these specimens, which made the specific pieces of tissue weaker than the remaining portions. In *in vivo* conditions, localized weaknesses in specific areas of the tissue tend to be compensated by stronger and more rigid portions, redistributing stress concentrations over longer distances and reducing the risks of compliant mechanical responses. On the contrary, localized defects tend to emerge much more in laboratory setups, where the samples are only sub-mm thick and have a width of just a few dozen millimeters (Tables S2-S3). Secondly, our analysis would certainly benefit from a larger number of FL samples and a deeper statistical analysis. However, coming from human donors, the number of FL samples for research purposes was extremely limited and unsteady over time. This left us with a relatively small population of samples. With a larger number of specimens, especially for each decellularization group, a more comprehensive statistical analysis could have been carried out, providing additional support for the identification of outliers and a more thorough comparison of treatment-aggregated properties. The samples used in this study were deemed ineligible for transplant due to blood test positivity for systemic infection or autoptic evidence of neoplasia (Table S1). While these conditions are not expected to impact the ECM of FL tissues and thus their overall structural properties, different mechanical analyses involving *in situ* characterization[38] might be required to verify these conclusions. Lastly, material properties such as E and σ_{max} can help to describe the mechanical behavior at the macroscopic scale of the sample and, for this reason, are often extensively used in the literature[23,27–30,32]. Yet, both suffer from two main shortcomings: (1) they rely on over-simplifications of the irregular geometries and mechanical inhomogeneities, non-linearities, and anisotropies of the specimen, and (2) they do not allow to appreciate differences in the mechanical behavior at a smaller mesoscopic scale. With the employment of DIC, these limitations can be partially overcome, and the

mechanical behavior of the FL tissue can be investigated at a smaller scale, allowing to highlight also localized effects up to ultimate collapse.

The results from DIC also suggested that no notable differences arise when comparing the meso-mechanical (deformative) properties of native FL against decellularized samples. Yet, it is interesting to compare longitudinal strains obtained from DIC to the average engineering strains evaluated from the stress-strain tensile curves at σ_{max}. The former were found to be ~5% for NatJ4, ~4% for TRX F4, ~15% for SDS F3, ~7% for TnBP F3 (see Section 3.2). The latter were ~10%, ~8%, ~25%, ~18% (see Figure 4), respectively. These engineering values are in line with the strains at break reported in the literature[23]. Moreover, they hold the same relationship across different samples as obtained from DIC (TRX < Nat < TnBP < SDS), suggesting that we can use both DIC and standard tensile tests to evaluate the differences in the deformation properties of FL samples. Yet, in all samples the average engineering values tend to overestimate the strains obtained from full-field DIC measurements. This happens because the FL samples are not homogeneous, and we observed that strains can undergo intense redistributions within the sample volume, often localizing in the upper and lower extremities of the tissue in close proximity of the external constrains. We also observed the occurrence of localized deformations and lacerations close to the machine clamps, which explains why in the area monitored by DIC the strains exhibit lower values compared to the average engineering strains that are simply evaluated from the evolving distances between the machine clamps. Our results suggest that monitoring strains by full-field measurements can reveal strong inhomogeneities and localization effects, which cannot be appreciated by relying only on traditional average engineering strains. This in turn can affect the estimated values of macro-mechanical properties such as the elastic modulus. Hence, we suggest that further research efforts should be devoted at integrating traditional stress measurements from uniaxial tests to strain observations from DIC for a more reliable characterization of the tissue mechanical features.

5. Conclusions

In this work, we have carried out a mechanical characterization of FL samples from human dead donors to investigate their macro- and meso-mechanical properties under uniaxial tension. Both native samples and specimens treated with Triton X-100, SDS, and TnBP were investigated. From the uniaxial tests, we computed values of the ultimate strength σ_{max} and elastic modulus E. After removing outliers, we did not observe any statistically significant deterioration of the (macro-mechanical) properties for any of the investigated decellularization protocols. We also used Digital Image Correlation (DIC) analysis to monitor the strain distribution within the specimen surfaces, both in the main direction of collagen fibers as well as in the orthogonal direction. The analysis of DIC strains indicated that the (meso-mechanical) deformation properties of FL specimens under different chemical treatments does not show major differences, leading to comparable strain evolutions and maximum strain values, as well as Poisson ratios of the same order of magnitude. The application of DIC analysis also proved effective in highlighting that relying on average engineering strains can lead to over- or under-estimations of the actual tissue deformations, especially when strain localizations, lacerations, or slippage events are found to occur close to the extremities[37]. Overall, the results of our analysis suggest that none of the investigated decellularization treatments deteriorates the mechanical performance of FL tissues, and they can therefore be used in the clinical practice, at least from a mechanical point of view. Further research efforts might be needed to increase the statistical significance of the mechanical characterization increasing the number of investigated

samples, improve the experimental setup aiming to reduce the degree of lacerations close to the machine clumps, and integrate the DIC strain measurements with the stress measurements for a more accurate evaluation of stress-strain curves and macro-mechanical properties. Additional research on the histological and biophysical compatibility of the tissue upon decellularization would be also needed to validate the applicability of these chemical treatments in the clinical practice.

Author Contributions

A.C. Faini, A. Leone, E. Camusso: Extraction of FL tissues from human dead donors; Preparation of the tissues; Application of the decellularization protocols. F. Demontis, G. Loi, E. Mazzotti: Preparation of FL tissues for the mechanical tests; Measuring of geometrical properties. M. Reinoso Rodriguez: Uniaxial tensile tests. F. Vecchio: DIC acquisition and post-processing. F. Genzano Besso, C. Surace, G. Lacidogna: Supervision. D. Scaramozzino: Overall project supervision; Post processing of results; Writing of the paper draft. All authors contributed to discussions and were involved in the draft revision.

References

1. Blaudez, F., Ivanovski, S., Hamlet, S. & Vaquette, C. An overview of decellularisation techniques of native tissues and tissue engineered products for bone, ligament and tendon regeneration. *Methods* **171**, 28–40 (2020).
2. Vitali, M. *et al.* Direct fascia lata reconstruction to reduce donor site morbidity in endoscopic endonasal extended surgery: a pilot study. *Clinical Neurology and Neurosurgery* **144**, 59–63 (2016).
3. Gillies, H. Experiences with Fascia Lata Grafts in the Operative Treatment of Facial Paralysis. *Proceedings of the Royal Society of Medicine* **27**, 1372–1382 (1934).
4. Silan, F. *et al.* Cryopreserved fascia lata allograft use in surgical facial reanimation: a retrospective study of seven cases. *Maxillofacial Plastic and Reconstructive Surgery* **42**, 2 (2020).
5. Dwivedi, R. C., Sattar, R., Tsiropulous, G. & Repanos, C. Fascia lata graft closure of an enlarged tracheoesophageal puncture (TEP) after laryngectomy/laryngopharyngectomy. *Eur Arch Otorhinolaryngol* **276**, 2355–2359 (2019).
6. Burnett, A. L. Fascia Lata in Penile Reconstructive Surgery: A Reappraisal of the Fascia Lata Graft. *Plastic and Reconstructive Surgery* **99**, 1061 (1997).
7. Walter, A. J., Hentz, J. G., Magrina, J. F. & Cornella, J. L. Harvesting autologous fascia lata for pelvic reconstructive surgery: Techniques and morbidity. *American Journal of Obstetrics and Gynecology* **185**, 1354–1359 (2001).
8. Beyer, C. K. & Albert, D. M. The Use and Fate of Fascia Lata and Sclera in Ophthalmic Plastic and Reconstructive Surgery: The 1980 Wendell Hughes Lecture. *Ophthalmology* **88**, 869–886 (1981).
9. Ono, J. *et al.* Free Tensor Fascia Lata Flap and Synthetic Mesh Reconstruction for Full-Thickness Chest Wall Defect. *Case Reports in Medicine* **2013**, 914716 (2013).
10. Jang, Y. J., Wang, J. H., Sinha, V., Song, H. M. & Lee, B.-J. Tutoplast-processed fascia lata for dorsal augmentation in rhinoplasty. *Otolaryngology - Head and Neck Surgery* **137**, 88–92 (2007).
11. Crapo, P. M., Gilbert, T. W. & Badylak, S. F. An overview of tissue and whole organ decellularization processes. *Biomaterials* **32**, 3233–3243 (2011).
12. Lotze, M. T., Deisseroth, A. & Rubartelli, A. Damage associated molecular pattern molecules. *Clin Immunol* **124**, 1–4 (2007).
13. Badylak, S. F. & Gilbert, T. W. Immune response to biologic scaffold materials. *Seminars in*

Immunology **20**, 109–116 (2008).
14. O'Neill, J. D. *et al.* Decellularization of human and porcine lung tissues for pulmonary tissue engineering. *Ann Thorac Surg* **96**, 1046–1055; discussion 1055-1056 (2013).
15. Alshaikh, A. B. *et al.* Decellularization of the mouse ovary: comparison of different scaffold generation protocols for future ovarian bioengineering. *J Ovarian Res* **12**, 58 (2019).
16. Liao, J., Joyce, E. M. & Sacks, M. S. Effects of decellularization on the mechanical and structural properties of the porcine aortic valve leaflet. *Biomaterials* **29**, 1065–1074 (2008).
17. Huh, M.-I. *et al.* Generation of Femtosecond Laser-Cut Decellularized Corneal Lenticule Using Hypotonic Trypsin-EDTA Solution for Corneal Tissue Engineering. *J Ophthalmol* **2018**, 2590536 (2018).
18. Deeken, C. R. *et al.* Method of preparing a decellularized porcine tendon using tributyl phosphate. *J Biomed Mater Res B Appl Biomater* **96**, 199–206 (2011).
19. Kumar Kuna, V., Xu, B. & Sumitran-Holgersson, S. Decellularization and Recellularization Methodology for Human Saphenous Veins. *J Vis Exp* 57803 (2018) doi:10.3791/57803.
20. Neishabouri, A., Soltani Khaboushan, A., Daghigh, F., Kajbafzadeh, A.-M. & Majidi Zolbin, M. Decellularization in Tissue Engineering and Regenerative Medicine: Evaluation, Modification, and Application Methods. *Front Bioeng Biotechnol* **10**, 805299 (2022).
21. Badylak, S. F., Freytes, D. O. & Gilbert, T. W. Extracellular matrix as a biological scaffold material: Structure and function. *Acta Biomaterialia* **5**, 1–13 (2009).
22. Haugen, H. J., Lyngstadaas, S. P., Rossi, F. & Perale, G. Bone grafts: which is the ideal biomaterial? *Journal of Clinical Periodontology* **46**, 92–102 (2019).
23. Bonaldi, L., Fontanella, C. G., Stecco, C. & Berardo, A. Design, implementation and effectiveness of human fascia lata biomechanics for tissue engineering. *Journal of Biomechanics* **176**, 112369 (2024).
24. Gratz, C. M. TENSILE STRENGTH AND ELASTICITY TESTS ON HUMAN FASCIA LATA. *JBJS* **13**, 334 (1931).
25. Thomas, O. L., Morrison, C., Howard, L. & Oni, O. O. A. The biomechanical properties of fascia lata grafts: a preliminary study. *Injury* **29**, 227–228 (1998).
26. Derwin, K. A. *et al.* Regional variability, processing methods, and biophysical properties of human fascia lata extracellular matrix. *Journal of Biomedical Materials Research Part A* **84A**, 500–507 (2008).
27. Eng, C. M., Pancheri, F. Q., Lieberman, D. E., Biewener, A. A. & Dorfmann, L. Directional Differences in the Biaxial Material Properties of Fascia Lata and the Implications for Fascia Function. *Ann Biomed Eng* **42**, 1224–1237 (2014).
28. Pancheri, F. Q., Eng, C. M., Lieberman, D. E., Biewener, A. A. & Dorfmann, L. A constitutive description of the anisotropic response of the fascia lata. *Journal of the Mechanical Behavior of Biomedical Materials* **30**, 306–323 (2014).
29. Otsuka, S. *et al.* Site specificity of mechanical and structural properties of human fascia lata and their gender differences: A cadaveric study. *Journal of Biomechanics* **77**, 69–75 (2018).
30. Pukšec, M. *et al.* Biomechanical Comparison of the Temporalis Muscle Fascia, the Fascia Lata, and the Dura Mater. *Journal of Neurological Surgery Part B: Skull Base* **80**, 023–030 (2018).
31. De Campos Azevedo, C. I. *et al.* Proximal and mid-thigh fascia lata graft constructs used for arthroscopic superior capsule reconstruction show equivalent biomechanical properties: an in vitro human cadaver study. *JSES International* **5**, 439–446 (2021).
32. Bonaldi, L. *et al.* Mechanical Characterization of Human Fascia Lata: Uniaxial Tensile Tests from Fresh-Frozen Cadaver Samples and Constitutive Modelling. *Bioengineering* **10**, 226 (2023).
33. Chu, T. C., Ranson, W. F. & Sutton, M. A. Applications of digital-image-correlation techniques to experimental mechanics. *Experimental Mechanics* **25**, 232–244 (1985).
34. Palanca, M., Tozzi, G. & Cristofolini, L. The use of digital image correlation in the biomechanical area: a review. *International Biomechanics* **3**, 1–21 (2016).
35. Boyce, B. L., Grazier, J. M., Jones, R. E. & Nguyen, T. D. Full-field deformation of bovine

cornea under constrained inflation conditions. *Biomaterials* **29**, 3896–3904 (2008).
36. Bakhshaee, H., Young, J., Yang, J. C. W., Mongeau, L. & Miri, A. K. Determination of Strain Field on the Superior Surface of Excised Larynx Vocal Folds Using DIC. *Journal of Voice* **27**, 659–667 (2013).
37. Luyckx, T. *et al.* Digital image correlation as a tool for three-dimensional strain analysis in human tendon tissue. *Journal of Experimental Orthopaedics* **1**, 7 (2014).
38. Sednieva, Y., Viste, A., Naaim, A., Bruyère-Garnier, K. & Gras, L.-L. Strain Assessment of Deep Fascia of the Thigh During Leg Movement: An in situ Study. *Front. Bioeng. Biotechnol.* **8**, (2020).
39. Burgio, V. *et al.* Mechanical properties of animal ligaments: a review and comparative study for the identification of the most suitable human ligament surrogates. *Biomech Model Mechanobiol* **22**, 1645–1683 (2023).
40. Chavan, R., Kamble, N., Kuthe, C. & Sarnobat, S. On Mechanical Behavior and Characterization of Soft Tissues. *Biomedical Engineering and Computational Biology* **15**, 11795972241294115 (2024).
41. Lynch, H. A., Johannessen, W., Wu, J. P., Jawa, A. & Elliott, D. M. Effect of Fiber Orientation and Strain Rate on the Nonlinear Uniaxial Tensile Material Properties of Tendon. *Journal of Biomechanical Engineering* **125**, 726–731 (2003).
42. Cheng, V. W. T. & Screen, H. R. C. The micro-structural strain response of tendon. *J Mater Sci* **42**, 8957–8965 (2007).
43. Vergari, C. *et al.* True stress and Poisson's ratio of tendons during loading. *Journal of Biomechanics* **44**, 719–724 (2011).
44. Chernak, L. A. & Thelen, D. G. Tendon motion and strain patterns evaluated with two-dimensional ultrasound elastography. *Journal of Biomechanics* **45**, 2618–2623 (2012).
45. Gatt, R. *et al.* Negative Poisson's ratios in tendons: An unexpected mechanical response. *Acta Biomaterialia* **24**, 201–208 (2015).
46. Takaza, M., Moerman, K. M., Gindre, J., Lyons, G. & Simms, C. K. The anisotropic mechanical behaviour of passive skeletal muscle tissue subjected to large tensile strain. *Journal of the Mechanical Behavior of Biomedical Materials* **17**, 209–220 (2013).
47. Mohammadkhah, M., Murphy, P. & Simms, C. K. The in vitro passive elastic response of chicken pectoralis muscle to applied tensile and compressive deformation. *Journal of the Mechanical Behavior of Biomedical Materials* **62**, 468–480 (2016).
48. Elliott, D. M., Narmoneva, D. A. & Setton, L. A. Direct Measurement of the Poisson's Ratio of Human Patella Cartilage in Tension. *Journal of Biomechanical Engineering* **124**, 223–228 (2002).
49. Wang, C. C.-B., Deng, J.-M., Ateshian, G. A. & Hung, C. T. An Automated Approach for Direct Measurement of Two-Dimensional Strain Distributions Within Articular Cartilage Under Unconfined Compression. *Journal of Biomechanical Engineering* **124**, 557–567 (2002).
50. Wang, C. C.-B., Chahine, N. O., Hung, C. T. & Ateshian, G. A. Optical determination of anisotropic material properties of bovine articular cartilage in compression. *Journal of Biomechanics* **36**, 339–353 (2003).
51. Zhang, J. *et al.* Strain and mechanical behavior measurements of soft tissues with digital speckle method. *J Biomed Opt* **10**, 034021 (2005).
52. Piët, M. P. *et al.* The use of tri(n-butyl)phosphate detergent mixtures to inactivate hepatitis viruses and human immunodeficiency virus in plasma and plasma's subsequent fractionation. *Transfusion* **30**, 591–598 (1990).